SCIENCE CHINA
Technological Sciences

•Article•

March 2021 Vol.64 No.3: 673–679
https://doi.org/10.1007/s11431-020-1643-5

Three-dimensional hierarchical $Ca_3Co_4O_9$ hollow fiber network as high performance anode material for lithium-ion battery

GUAN ShouJie[1,2†], FAN QingLu[1,2†], LIU LiYing[1,2], LUO JunCai[2], ZHONG YiCheng[1,2], ZHAO WeiMin[3], HUANG ZhenCai[4] & SHI ZhiCong[1,2*]

[1]*Smart Energy Research Centre, School of Materials and Energy, Guangdong University of Technology, Guangzhou 510006, China;*
[2]*Guangdong Engineering Technology Research Center for New Energy Materials and Devices, Guangzhou 510006, China;*
[3]*College of Chemical Engineering and Safety, Binzhou University, Binzhou 256503, China;*
[4]*Hangzhou LIAO Technology Co., Ltd., Hangzhou 310000, China*

Received March 28, 2020; accepted May 18, 2020; published online October 20, 2020

Transition metal oxides have high specific capacity as anode materials for lithium-ion battery. But aggregation of particles and volume expansion during lithiation/delithiation restrict their application. In this work, a three-dimensional hierarchical $Ca_3Co_4O_9$ hollow fiber network assembled by nanosheets is prepared by an electrospinning combined with heat treatment method to overcome these issues and to boost its lithium storage performance. As-synthesized sample possesses excellent cyclic stability (578.6 mA h g^{-1} at 200 mA g^{-1} after 500 cycles) and rate performance (293.5 mA h g^{-1} at 5000 mA g^{-1}), much better than those of commercial Co_3O_4. Furthermore, the fast kinetics of the three-dimensional $Ca_3Co_4O_9$ hollow fiber network is also confirmed by the variable scan rates CV tests and the EIS measurements, which is dedicated to the specific hierarchical hollow fiber network structure that provides shorter ion transport distances and higher electrical conductivity. This work supplies a universal approach to improve the electrochemical performance of transition metal oxides for lithium ion batteries.

lithium ion battery, anode material, cobalt oxides, electrospinning, hierarchical structure

Citation: Guan S J, Fan Q L, Liu L Y, et al. Three-dimensional hierarchical $Ca_3Co_4O_9$ hollow fiber network as high performance anode material for lithium-ion battery. Sci China Tech Sci, 2021, 64: 673–679, https://doi.org/10.1007/s11431-020-1643-5

1 Introduction

Lithium-ion batteries (LIBs) are the most popular power sources for consumer electronics, electric vehicles, and future smart grids [1,2]. With the rapid development of cathode materials, anode materials and electrolyte, LIBs deliver more and more energy and power for devices [3–5]. Although graphite is the most widely used anode material for LIBs, it exhibits very limited theoretical capacity (372 mA h g^{-1}) [6]. Therefore, transition metal oxides (TMs), such as Fe_3O_4, Co_3O_4, MnO_2, CuO, $ZnMn_2O_4$ and $ZnFe_2O_4$, are considered as most promising anode materials due to high theoretical capacity and low cost [7–12]. In addition, TMs also delivered better safety owing to the higher lithium intercalation voltage [13]. Among them, the reversible theoretical specific capacity of Co_3O_4 (896 mA h g^{-1}) is more than twice that of graphite. But it does suffer rapid capacity decay and low rate performance caused by electrode pulverization, low conductivity and large volume expansion during charge and discharge [14,15].

c axis oriented layered oxide $Ca_3Co_4O_9$, with Co ions partially replaced by low-cost and environmentally friendly Ca ions, is a potential anode material for LIBs. Even though the generated CaO inactive matrix during first discharge process of this Ca substituted material could serve as the *in situ* SEI and can also mitigate the volume expansion during

†These authors contributed equally to this work.
*Corresponding author (email: zhicong@gdut.edu.cn)

charge and discharge process [16,17], it still faces challenges to improve the long cycling stability of $Ca_3Co_4O_9$. One of the main reasons is that the commonly used solid reaction method cannot produce suitable and uniform particles, which will go against the transportation of ions and electrons in the material [18]. Although homo-dispersed $Ca_3Co_4O_9$ nanoparticles have been prepared by sol-gel method in some literature, the aggregation of metallic nanoparticles and the large volume change during charge-discharge cycling still severely restrict the cyclic stability [16,19–22]. In addition to optimizing synthesis process, researchers also tried to dope with K, Cr, Fe and Mn elements [23,24], which has been considered as an effective strategy to increase the reaction active and electronic conductivity. Zhang et al. [25] prepared layered $Bi_2Ca_3Co_2O_9$ composite anode materials using the conventional solid-state reaction and flux method by partially replacing the Co ion with Bi ion for lithium-ion battery.

In our work, the three-dimensional $Ca_3Co_4O_9$ hollow fibers assembled by nanosheets were prepared by electrospinning combined with heat treatment, and a superior electrochemical performance was obtained due to the novel hierarchical structure. The hollow fiber structure can restrain the volume expansion, relieve agglomeration of metallic nanoparticles and provide large contact areas between electrolyte and electrode [26]. Meanwhile, the nanosheets attached to the hollow fibers are beneficial to shorten the transport distances of Li ion and electron in solid phase [27]. In addition, the pseudocapacitive characteristic of the three dimensional $Ca_3Co_4O_9$ hollow fiber network provides high-rate performance for lithium ions storage. Hence, the $Ca_3Co_4O_9$ displays superior cycling stability and rate property for Li-ion storage.

2 Experimental procedure

2.1 Materials preparetion

2.1.1 Synthesis of $Ca(NO_3)_2$

In a typical synthesis, 5.1 g $CaCO_3$ (M_w=100.09, Aladdin) was dissolved in 100 mL HNO_3 solution (1 M, M_w=63.01) and stirred (magnetic stirring apparatus, Yushen ZNCL-TS68*75) at 90°C until the liquid fully evaporated. The left powder was dried in a vacuum oven (vacuum drying oven, Suopu DZF-6020) at 150°C for 12 h to obtain $Ca(NO_3)_2$.

2.1.2 Preparation of precursor fibers

The precursor fibers were synthesized as follows. 0.472 g $Co(NO_3)_2{\cdot}6H_2O$ (M_w=291.03, Aladdin) and 0.204 g $Ca(NO_3)_2$ were added into the mixed solution including 10 mL dimethyl formamide (DMF, M_w=79.12, Sigma-Aldrich, USA) and 1 g polyacrylonitrile (PAN, M_w=150000, Sigma-Aldrich, USA). The precursor solution with suitable viscosity was obtained after continuous stirring. By electrospinning (electrospinning device, home-made) the precursor solution, precursor fibers were collected on a grounded stainless steel foil. The flow rate of the precursor solution and the collector distance were fixed at 5 μL/min and 12 cm, respectively. A high voltage of 18 kV was loaded to the needle for electrospinning.

2.1.3 Preparation of $Ca_3Co_4O_9$ hollow fiber network

As-collected fibers were calcined at 150°C for 3 h, then 350°C for 3 h, and 650°C for 6 h at last (a ramp rate of 2°C per minute) under air atmosphere. Then the products were dried in a vacuum oven at 80°C for 12 h.

2.2 Material characterizations

The X-ray diffraction (XRD, Rigaku D/max-2200/PC, Cu Kα, λ=0.1541 nm) was used to determine the crystal structure. The structures and morphologies were investigated through field-emission scanning electron microscopy (FESEM, S-3400N). The course of crystallization was investigated by Thermo-Gravimetric Analysis (TGA) from 30 to 800°C at the heating rate of 10°C min^{-1} under air atmosphere.

2.3 Electrochemical measurements

The electrochemical performance was tested using CR2032 coin cells, which were assembled in an argon-filled glove box. The working electrode (copper foil as current collector) was prepared using a typical method by mixing $Ca_3Co_4O_9$ hollow fibers (or commercial Co_3O_4) with carbon black and PVDF (as the binder) in the weight ratio of 7:2:1 with *N*-methyl-2-pyrrolidinone (NMP) as solvent. The mass loading of active material was controlled to be in the range from 1.5 to 2.0 mg cm^{-2}. The Celgard 2300 membrane was used as separator and Li foil was used as counter electrode. The electrolyte was 1 mol L^{-1} $LiPF_6$ dissolved in ethylene carbonate/diethyl carbonate (1:1 *v*/*v*) with 5 wt% fluoroethylene carbonate (FEC). Galvanostatic charge/discharge measurements were carried out using a LAND CT2001A multichannel battery test system at a voltage range of 0.05–3 V. The electrochemical workstation (Solartron 1287/1260) was used to collect the data of cyclic voltammetry (CV) curves in the voltage range of 0.05–3 V and electrochemical impedance spectra (EIS, the frequency range from 0.01 Hz to 100 kHz).

3 Results and discussion

Figure 1(a) depicts the detailed synthetic process of $Ca_3Co_4O_9$ hollow fiber network. Firstly, calcium source, cobalt source and polymer were dissolved in organic solvent to form precursor solution. Then, solid fibers were prepared

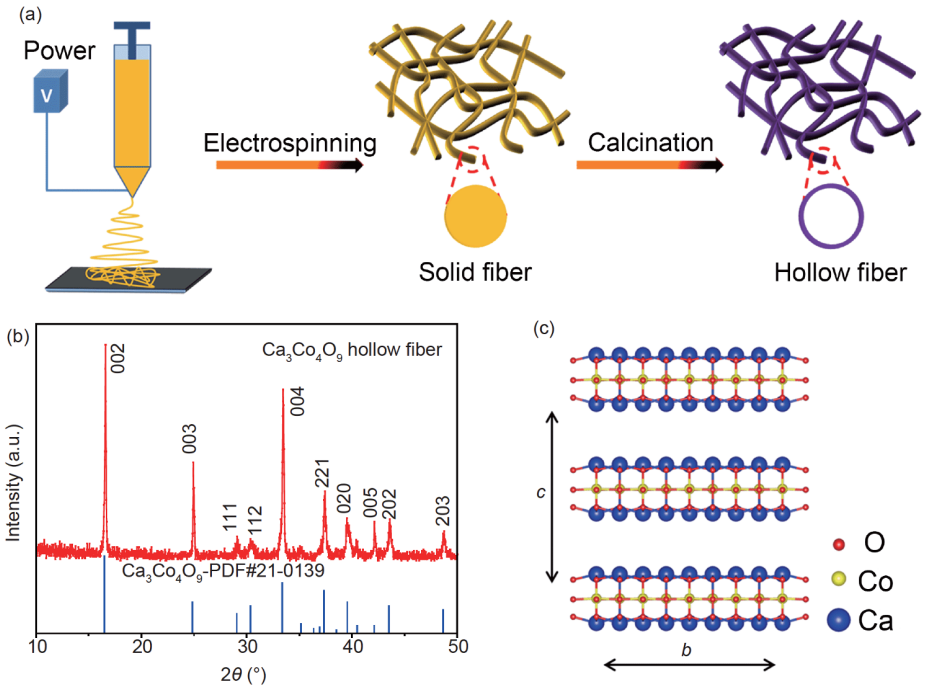

Figure 1 (Color online) Schematic illustration of the formation process of $Ca_3Co_4O_9$ hollow fiber network (a); XRD patterns of $Ca_3Co_4O_9$ hollow fiber network (b) and the crystal structure of $Ca_3Co_4O_9$ (c).

by electrospinning combined with heat treatment to obtain a hollow fiber network. The obtained precursor was heated step by step with different temperatures to get the final sample in order to maintain the structure of hollow fiber network and the uniform size of particles. The XRD pattern of as-prepared sample (Figure 1(b)) can be well indexed to PDF card No.21-0139, similar to the reported $Ca_3Co_4O_9$ [19]. In addition, the high peak intensity demonstrates the well-crystallinity of $Ca_3Co_4O_9$ hollow fibers. Figure 1(c) shows the crystal structure of $Ca_3Co_4O_9$ with countless rock-salt-type layers of [CaO-CoO_2-CaO] units in the *c* axis direction [16]. High electronic conductivity due to the unique layered structure of $Ca_3Co_4O_9$ makes it more suitable as anode material for LIBs than Co_3O_4 with spinel structure [16].

To determine the suitable calcination temperature, TGA/DSC measurement was carried out. According to the results in Figure 2(b), the weight loss between 20°C and 240°C may be caused by the volatilization of water; and the large weight loss between 240°C and 440°C can be attributed to the decomposition of DMF and PAN, with most parts of the precursor; with increased temperature, a small weight loss appears between 440°C and 650°C and then maintains constant even up to 800°C. Therefore, the calcination temperature for $Ca_3Co_4O_9$ was determined at 650°C [28]. The overall morphology of $Ca_3Co_4O_9$ did not change a lot before and after calcination, the similar fiber networks can be clearly seen in Figure 2(c) and (a). While the fibers presented unique micro morphology after calcination with ultrathin and uniform nanosheets. Meanwhile, the hollow structure of these fibers was also observed (Figure 2(e)). The formation mechanism can be attributed to that the polymer in the precursor fibers was oxidized to CO_2 and volatilized rapidly, and calcium and cobalt sources accumulated on the tube surface during the volatilization of polymer [29]. EDS mapping in Figure 2(f) indicates the existence and uniform distribution of Ca, Co and O elements on the surface of these nanosheets.

To evaluate the electrochemical properties of this hollow fiber network, CV and galvanostatic charge and discharge tests were performed. Figure 3(a) shows the CV profiles for $Ca_3Co_4O_9$ at different cycle between 0.05 and 3 V at a scanning rate of 0.1 mV s^{-1}. In the first cathodic scanning, an obvious reduction peak is observed at 0.665 V, which is ascribed to the formation of the Co nano-clusters, CaO matrix and pseudo-amorphous Li_2O [16]. And the two inconspicuous peaks (at 1.768, 1.033 V) can be attributed to the irreversible embedding of lithium into $Ca_3Co_4O_9$ [20]. In the process of anodic scanning, the formation of α-CoO and Co_3O_4 generated two peaks at 1.309 V and at 2.031 V [22]. It is worth noticing that the CV curves of $Ca_3Co_4O_9$ hollow fiber electrode were almost coincident with that of commercial Co_3O_4 anode (Figure 3(b)) in the subsequent cycles. Nevertheless, the CV curves of commercial Co_3O_4 do not overlap well, which may be caused by the aggregation of particle and the pulverization of the electrode in the process of cycling [15]. Comparing the positions of oxidation and reduction peaks for the two materials, the lower charging voltage for $Ca_3Co_4O_9$ can be observed, implying more sui-

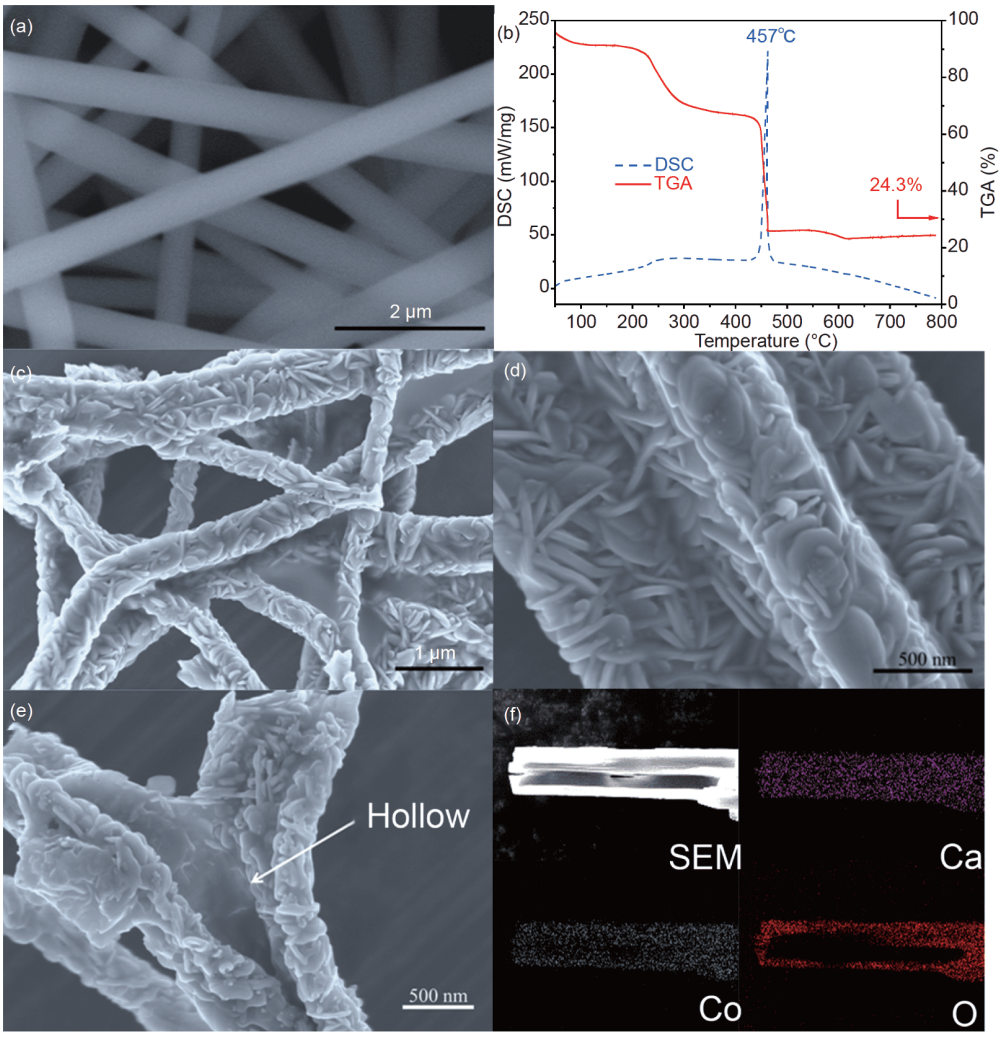

Figure 2 (Color online) SEM image of precursor fibers (a); TGA/DSC digital image of precursor fibers (b); SEM images of $Ca_3Co_4O_9$ hollow fibers (c)–(e); SEM image and the corresponding EDS mappings for $Ca_3Co_4O_9$ nanosheets (f).

table for LIBs as anode material. The above mechanism is consistent with previous reported one [22].

$$12Li + Ca_3Co_4O_9 \rightarrow 3CaO + 4Co + 6Li_2O$$

(the first discharge),

$$3Co + 4LiO_2 \rightleftharpoons Co_3O_4 + 8Li$$

(subsequent charge/discharge).

Figure 3(c) shows the representative galvanostatic charge/discharge profiles of $Ca_3Co_4O_9$ hollow fiber electrode at the 1st, 2nd, 3rd, 5th and 200th cycle at the current of 200 mA g^{-1}. The initial specific discharge capacity for $Ca_3Co_4O_9$ is 1199 mA h g^{-1}, which exceeds the theoretical capacity (643.3 mA h g^{-1}) but less than that of Co_3O_4. Though $Ca_3Co_4O_9$ has a high irreversible capacity at the first cycle, the formed irreversible components have been confirmed to be beneficial to prevent the destruction of structures and sustain the cyclic stability [15,16]. Comparing the charge and discharge curves at different cycles of $Ca_3Co_4O_9$ and Co_3O_4 in Figure 3(c) and (d), the closer curves can be observed for $Ca_3Co_4O_9$, which indicates the better capacity retention. The long cycling performances of $Ca_3Co_4O_9$ hollow fiber electrode and commercial Co_3O_4 electrode at 200 mA g^{-1} are described in Figure 3(e). It still maintained at 578.6 mA h g^{-1} after 500 cycles for $Ca_3Co_4O_9$, much higher than that of commercial Co_3O_4 electrode (311.5 mA h g^{-1} after 200 cycles at 200 mA g^{-1}). The superior cyclic stability of $Ca_3Co_4O_9$ can be attributed to the three-dimensional hollow fiber network, which can restrain the volume expansion and aggregation of particles during cycling [30]. As shown in Figure 3(e), the capacity of the battery fluctuated up and down during cycling. Lithium plating, SEI growth, transition metal dissolution, mechanical cracking, and electrolyte depletion, etc., usually lead to the capacity attenuation of electrode materials. While the increasing of capacity is due to the cracking of active material particles, which produces much electrochemical active interface for lithium storage at low voltage area. Rate properties are described in Figure 4(a). It can be seen that the rate performance of

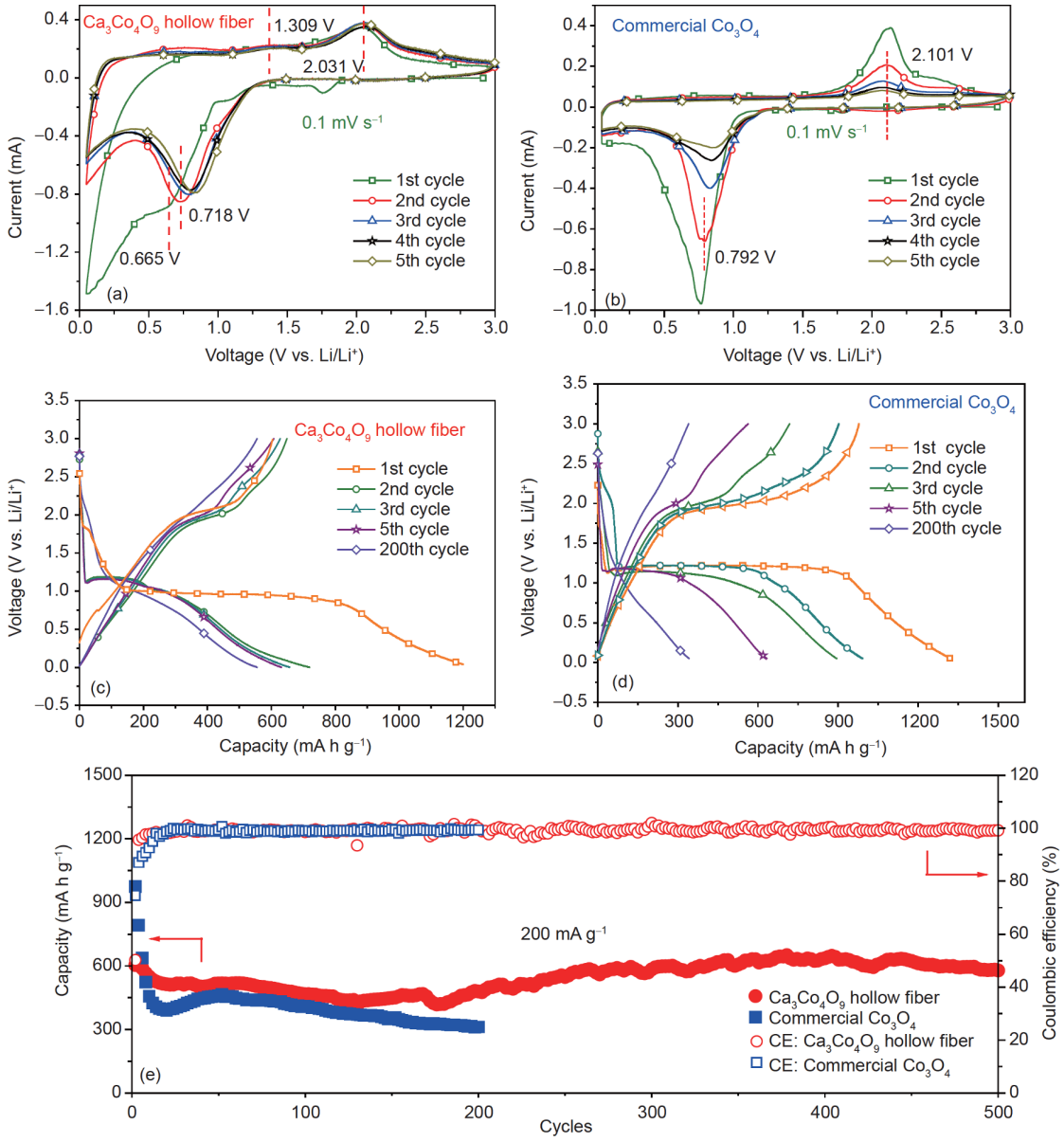

Figure 3 (Color online) CV profiles of $Ca_3Co_4O_9$ hollow fiber electrode (a) and commercial Co_3O_4 electrode (b) between 0.05 and 3 V (vs. Li^+/Li) at a scanning rate of 0.1 mV s^{-1}. Galvanostatic charge/discharge profiles of $Ca_3Co_4O_9$ hollow fiber electrode (c) and commercial Co_3O_4 electrode (d) at 200 mA g^{-1}. (e) Long cycling performances of $Ca_3Co_4O_9$ hollow fiber electrode and commercial Co_3O_4 electrode at current of 200 mA g^{-1}.

$Ca_3Co_4O_9$ hollow fiber electrode is much more outstanding than that of commercial Co_3O_4 electrode. With the increase of current densities, the specific charge capacities of $Ca_3Co_3O_9$ are always higher than those of Co_3O_4, though $Ca_3Co_4O_9$ has a lower initial specific discharge capacity. When the current density up to 5000 mA g^{-1}, the $Ca_3Co_4O_9$ still can deliver specific charge capacity of 293.5 mA h g^{-1}, while it is only 133.8 mA h g^{-1} for commercial Co_3O_4. In order to explore the reason for higher rate performance, the CV profiles at various sweep rates for $Ca_3Co_4O_9$ and commercial Co_3O_4 were measured, as shown in Figure 4(c) and (d). Meanwhile, the linear relationship of log(v) and log(i) profiles are given in Figure 4(e), which is based on the equation $i = a \cdot v^b$ (i is the peak current, v is the corresponding sweep rate) [31]. When b value is in the range of 0.5–1.0, the sample exhibits the characteristic of pseudocapacitance which has been proven to be beneficial to the rapid transmission of ions [32]. The results demonstrate that the $Ca_3Co_4O_9$ hollow fibers (b = 0.804) have a higher capacitive kinetics than commercial Co_3O_4 (b = 0.306) due to the large specific surface of the microcosmic nanosheet structure. The large specific surface of $Ca_3Co_4O_9$ nanosheets can provide enough active interfaces for oxidation-reduction reaction and shorten the ions transport distance in the material, meanwhile, the three-dimensional hollow fiber network can also accelerate the electron transmission among the overall

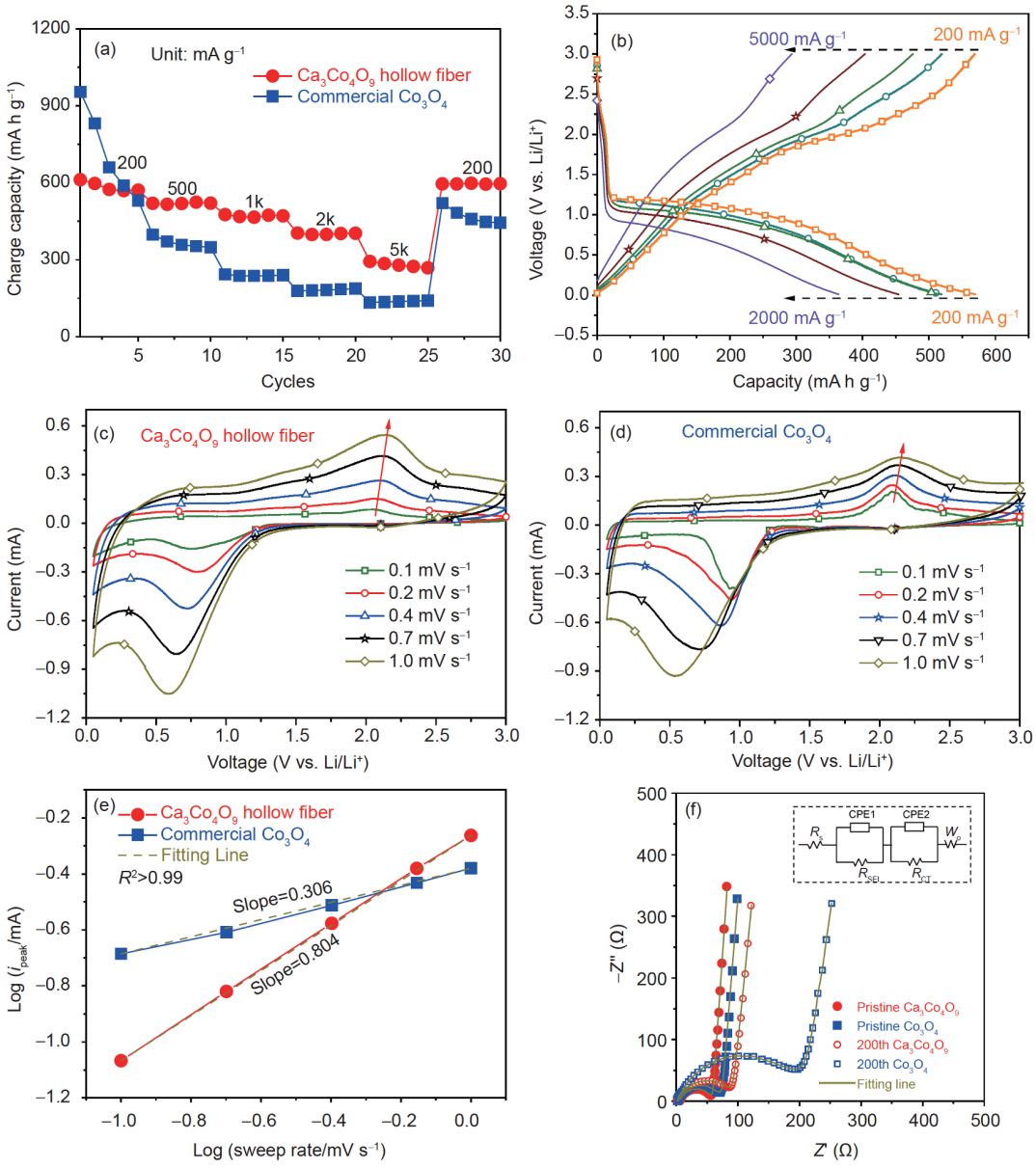

Figure 4 (Color online) Rate performances of $Ca_3Co_4O_9$ hollow fiber electrode and commercial Co_3O_4 electrode (a), discharge profiles of $Ca_3Co_4O_9$ hollow fiber electrode at different current densities (b). CV curves at different scan rates from 0.1 to 1.0 mV s^{-1} for $Ca_3Co_4O_9$ hollow fiber electrode (c) and commercial Co_3O_4 electrode (d). The linear relationship of the log(v) and log(i) for the $Ca_3Co_4O_9$ hollow fiber electrode and commercial Co_3O_4 electrode (e). EIS data for $Ca_3Co_4O_9$ and Co_3O_4 before and after 200 cycles (f), the inset picture is the equivalent circuit for the impedance spectra.

electrode.

Furthermore, the kinetics for two samples was also further discussed by EIS (Figure 4(f)). In Figure 4(f), Each Nyquist curve of EIS consist of two highly overlapped semicircles and a sloped line, which can be fitted by an equivalent circuit including two series connected (parallel RC circuit) and a Warburg impedance element as shown in the inset. The semicircle at high frequency represents the Li^+ migration through the solid electrolyte interface (SEI) on the surface of the anode materials (including R_{SEI} and CPE1 elements), and the starting point of which represents the electrolyte resistance (R_s). While the semicircle at medium frequency represents the charge transfer process (including R_{ct} and CPE2 elements). The slope line at low frequency attributes to the Warburg impedance (Wo) representing the Li^+ diffusion in anode material [3]. The $Ca_3Co_4O_9$ hollow fiber electrode manifested smaller charge-transfer resistance in contrast to the commercial Co_3O_4 electrode. The $Ca_3Co_4O_9$ hollow fiber electrode generated CaO matrix, increasing the impedance after 200 cycles [21]. But the impedance of commercial Co_3O_4 electrode increased significantly after 200 cycles, which may be caused by the aggregation of particle and large volume expansion [9]. It is worth noting that a limited increase in impedance of $Ca_3Co_4O_9$ hollow fiber electrode can

be attributed to the unique hollow fiber network, which can relieve the volume expansion and maintain good contact between active material and current collector during cycling process.

4 Conclusions

In summary, we successfully synthesized the three-dimensional hierarchical $Ca_3Co_4O_9$ with hollow fibers and nanosheets by electrospinning combining with heat treatment. The unique hierarchical structure is beneficial to relieve volume expansion, prevent aggregation of Co nanoclusters and shorten the transport distance of lithium ions and electrons. Compared with commercial Co_3O_4, $Ca_3Co_4O_9$ hollow fiber electrode shows superior cycling performance with specific charge capacity of 578.6 mA h g^{-1} after 500 cycles at 200 mA g^{-1} with almost no apparent decay. Also, the $Ca_3Co_4O_9$ hollow fiber electrode presents a higher reversible specific capacity of 293.5 mA h g^{-1} at 5000 mA g^{-1} due to the favorable kinetics than commercial Co_3O_4 material. The defined structure design of hollow fiber network in this paper is as an effective way to improve electrochemical properties of electrode materials for chemical power sources.

This work was supported by the National Natural Science Foundation of China (Grant No. 21673051), and the Department of Science and Technology of Guangdong Province, China (Grant No. 2019A050510043). Fan QL acknowledges the financial support from China Scholarship Council.

1 Shi S Q, Gao J, Liu Y, et al. Multi-scale computation methods: Their applications in lithium-ion battery research and development. Chin Phys B, 2016, 25: 018212
2 Cheng Y, Ke X, Chen Y, et al. Lithiophobic-lithiophilic composite architecture through co-deposition technology toward high-performance lithium metal batteries. Nano Energy, 2019, 63: 103854
3 Fan Q, Yang S, Liu J, et al. Mixed-conducting interlayer boosting the electrochemical performance of Ni-rich layered oxide cathode materials for Lithium ion batteries. J Power Sources, 2019, 421: 91–99
4 Chen Y, Ke X, Cheng Y, et al. Boosting the electrochemical performance of 3D composite lithium metal anodes through synergistic structure and interface engineering. Energy Storage Mater, 2020, 26: 56–64
5 Ke X, Liang Y, Ou L, et al. Surface engineering of commercial Ni foams for stable Li metal anodes. Energy Storage Mater, 2019, 23: 547–555
6 Deng Y, Zhang Q, Shi Z, et al. Synergies of the crystallinity and conductive agents on the electrochemical properties of the hollow Fe_3O_4 spheres. Electrochim Acta, 2012, 76: 495–503
7 Liu F, Xiao Y, Liu Y, et al. Mesoporous MnO_2 based composite electrode for efficient alkali-metal-ion storage. Chem Eng J, 2020, 380: 122487
8 Deng Y, Tang S, Zhang Q, et al. Controllable synthesis of spinel nano-$ZnMn_2O_4$ via a single source precursor route and its high capacity retention as anode material for lithium ion batteries. J Mater Chem, 2011, 21: 11987–11995
9 Deng Y, Zhang Q, Tang S, et al. One-pot synthesis of $ZnFe_2O_4$/C hollow spheres as superior anode materials for lithium ion batteries. Chem Commun, 2011, 47: 6828–6830
10 Zhang Q, Shi Z, Deng Y, et al. Hollow Fe_3O_4/C spheres as superior lithium storage materials. J Power Sources, 2011, 197: 305–309
11 Wang J, Zheng B, Qiao Z, et al. Construct 3D porous hollow Co_3O_4 micro-sphere: A potential oxidizer of nano-energetic materials with superior reactivity. Appl Surf Sci, 2018, 442: 767–772
12 Huang S M, Luo J, Yuan W, et al. Three-dimensional porous composite framework assembled with CuO microspheres as anode current collector for lithium-ion batteries. Sci China Technol Sci, 2019, 62: 70–79
13 Zhang J, Yu A. Nanostructured transition metal oxides as advanced anodes for lithium-ion batteries. Sci Bull, 2015, 60: 823–838
14 Han T, Ding Y, Chen Y, et al. A novel spring-structured coaxial hierarchical SiO_2@Co_3O_4 nanowire as a lithium-ion battery anode and its *in situ* real-time lithiation. Nanotechnology, 2020, 31: 035401
15 Wang L, Yuan Y F, Chen Q, et al. Construction of Co_3O_4 three-dimensional mesoporous framework structures from zeolitic imidazolate framework-67 with enhanced lithium storage properties. Nanotechnology, 2019, 30: 435402
16 Kim D W, Ko Y D, Park J G, et al. Formation of lithium-driven active/inactive nanocomposite electrodes based on $Ca_3Co_4O_9$ nanoplates. Angew Chem Int Ed, 2007, 46: 6654–6657
17 Xu X, Wu P, Li Q, et al. Realizing stable lithium and sodium storage with high areal capacity using novel nanosheet-assembled compact CaV_4O_9 microflowers. Nano Energy, 2018, 50: 606–614
18 Masset A C, Michel C, Maignan A, et al. Misfit-layered cobaltite with an anisotropic giant magnetoresistance: $Ca_3Co_4O_9$. Phys Rev B, 2000, 62: 166–175
19 Zhou S, Tao Z, Liu J, et al. Bricklike $Ca_9Co_{12}O_{28}$ as an active/inactive composite for lithium-ion batteries with enhanced rate performances. ACS Omega, 2019, 4: 6452–6458
20 Kim D W, Ko Y D, Park J S, et al. Electrochemical performance of calcium cobaltite nano-plates. J Nanosci Nanotech, 2009, 9: 4056–4060
21 Prasoetsopha N, Pinitsoontorn S, Kamwanna T, et al. Improvement of electrochemical properties of $Ca_3Co_4O_9$ as anode materials for lithium-ion batteries by cr doping. J Solid State Electrochem, 2015, 19: 1197–1202
22 Zhu X B, Chou S L, Wang L, et al. Self-oriented $Ca_3Co_4O_9$ thin film as an anode material for enhanced cycling stability of lithium-ion batteries. Electrochem Solid-State Lett, 2009, 12: A176
23 Cao J, Liu H, Xie J, et al. Effect of K-doping on the electrochemical performance of $Ca_3Co_4O_9$ anode for Li-ion batteries. J Mater Sci Tech, 2010, 26: 669–672
24 Prasoetsopha N, Pinitsoontorn S, Fan S, et al. Enhancement of electrochemical properties of $Ca_3Co_4O_9$ as anode materials for lithium-ion batteries by transition metal doping. Ionics, 2016, 23: 395–403
25 Zhang Y, Wang S L, Liu A P, et al. Layered $Bi_2Ca_3Co_2O_9$ composite as anode material for lithium-ion battery. Appl Phys A, 2010, 98: 281–284
26 Huang X, Liu J, Huang Z, et al. Flexible free-standing sulfurized polyacrylonitrile electrode for stable Li/Na storage. Electrochim Acta, 2020, 333: 135493
27 Pomerantseva E, Bonaccorso F, Feng X, et al. Energy storage: The future enabled by nanomaterials. Science, 2019, 366: eaan8285
28 Wang L, Yu Y, Chen P C, et al. Electrospinning synthesis of C/Fe_3O_4 composite nanofibers and their application for high performance lithium-ion batteries. J Power Sources, 2008, 183: 717–723
29 Mai L, Xu L, Han C, et al. Electrospun ultralong hierarchical vanadium oxide nanowires with high performance for lithium ion batteries. Nano Lett, 2010, 10: 4750–4755
30 Yu P C, Yuan Y C. One-step synthesis of robust carbon nanotube foams with ultrahigh surface area for high-performance lithium ion battery. Sci China Tech Sci, 2019, 62: 464–471
31 Augustyn V, Simon P, Dunn B. Pseudocapacitive oxide materials for high-rate electrochemical energy storage. Energy Environ Sci, 2014, 7: 1597
32 Gan Q, He H, Zhu Y, et al. Defect-assisted selective surface phosphorus doping to enhance rate capability of titanium dioxide for sodium ion batteries. ACS Nano, 2019, 13: 9247–9258